Article ID: 1003－6326(2003)01－0050－05

Fatigue crack propagation behavior of K40S cobalt-base superalloy at elevated temperature①

YANG Fu-min (杨富民)[1], SUN Xiao-feng(孙晓峰)[1], GUAN Heng-rong (管恒荣)[1], DENG Wu-li (邓午立)[2], LIU Fang (刘 芳)[2], HU Zhuang-qi (胡壮麒)[1]
(1. Institute of Metal Research, Chinese Academy of Sciences, Shenyang 110016, China;
2. Shenyang Aero-engine Research Institute, Shenyang 110034, China)

Abstract: Fatigue crack propagation behavior of K40S cobalt-base superalloy under ambient atmosphere at 700 ℃ and 900 ℃ was investigated. The detailed fatigue crack propagation and fracture mechanism under the alternating loads were studied. The results show that, there is a defined threshold for K40S alloy at elevated temperatures. The fatigue threshold is 23.9 MPa·$m^{1/2}$ at 700 ℃ and 12 MPa·$m^{1/2}$ at 900 ℃. The significant decrease of the threshold with increasing temperature is associated with the oxidation induced embrittlement at crack tip. Observation on the fatigue fracture surfaces indicates a ductile fracture mechanism related to the fatigue crack growth.

Key words: cobalt-base superalloy; fatigue crack propagation; fatigue threshold; ductility
CLC number: TG 146; TG 111 **Document code:** A

1 INTRODUCTION

Due to a good combination of high temperature rupture stress and excellent hot corrosion resistance after prolonged exposure, cast cobalt-base superalloys are widely used in many military and commercial engines as high temperature structural components[1, 2].

K40S alloy is a cobalt-base superalloy developed from the conventional X-40 cobalt-base alloy by adding B element and modifying the contents of Si, Mn, etc. Compared with X-40 alloy, it shows superior high-temperature strength, elongation and corrosion resistance[3, 4].

In many cases of failure analysis of aero-engines, the mechanical fatigue fracture is very common. Fracture mechanics has been used to describe the fatigue behavior of metallic materials for a long time and a considerable amount of literature can be found in this field[5-8].

The related fatigue damage mechanism proposed by Soboyejo et al[6] is that the accumulation of microplasticity in the form of coarse slip bands is the major mechanism in the initiation stage. While unzipping of microcracks along some preferential slip bands contributes to the main crack propagation.

In order to correlate the crack growth rate, da/dN, with the crack driving force, i.e., the stress intensity factor range, ΔK, the Paris equation is commonly used[9]:

$$da/dN = c(\Delta K)^m \quad (1)$$

where c and m are material parameters, and $\Delta K = K_{max} - K_{min}$.

For the compact-tension (CT) specimens used in this study, the stress intensity factor range take the form as follows[10]:

$$\Delta K = \frac{\Delta p(2+\alpha)}{B\sqrt{W}(1-\alpha)^{3/2}}(0.886+4.64\alpha-13.32\alpha^2+14.72\alpha^3-5.6\alpha^4) \quad (2)$$

where Δp is the load range; B is the sample thickness; $\alpha = a/W$, here a is the crack length, W is the sample width.

In the mid-growth rate regime, namely the commonly observed linear range of the fatigue crack propagation in materials, the Paris law can closely describe the fatigue kinetics[7, 11], and the exponent, m, can be determined experimentally. At both low and high crack growth ranges, there are nonlinear behavior of $\lg(da/dN)$ versus the stress intensity factor range (ΔK). Other fatigue models based on the modification of Eqn. (1) have the same applicability in the near-threshold stage for design purposes[12, 13].

Much attention has been paid on fatigue crack propagation behavior of nickel-base and iron-base superalloys. But for cobalt-base superalloy, it is only a little. The aim of this study is to investigate the fatigue crack propagation (FCP) behavior of K40S cobalt-base superalloy and to evaluate the fatigue crack growth resistance to guide the engine design and material selection.

2 EXPERIMENTAL

① **Received date:** 2002－04－01; **Accepted date:** 2002－10－08
Correspondence: YANG Fu-min, yfm110@263.net

K40S alloy was prepared in a conventional vacuum induction furnace. The nominal composition of the alloy is 25.5Cr, 10.5Ni, 7.5W, 0.5C, 0.8Si, 0.8Mn and 0.004B (mass fraction, %), with the balanced cobalt. Compact-tension (CT) configuration for the samples was selected for this study. All samples were cut from the cast plates and machined into the geometry, according to ASTM standards. The thickness of the CT specimens is 3.5 mm. In order to facilitate precracking, the radius of the notch root section is no more than 0.08 mm. Surface finishing (the arithmetical average deviation from the mean plane is better than 0.8 μm) was done, including the two loading holes. FCP tests were performed using a 810 electro-servohydraulic materials testing system (MTS) equipped with a 100 kN load cell and a furnace, in which the temperature was controlled with three platinum-rhodium thermocouples. Tests were conducted under constant cyclic loading at a frequency of 30 Hz at room temperature and at elevated temperature, 700 ℃ and 900 ℃, in ambient atmosphere. The stress ratio R was 0.1. A sinusoidal waveform was used.

Specimens were precracked at room temperature (RT). The crack was initiated at $\Delta K = 37.95$ MPa·$m^{1/2}$. The stress intensity was progressively reduced in steps in such a way that ΔK was never less than 80% of the previous ΔK. Finally, about 0.5 mm-long crack were grown under a $\Delta K = 7.8$ MPa·$m^{1/2}$ to provide a common starting point. This resulted in a final precrack length, excluding the machined notch, of approximately 2.5 mm. This process was rapid and provided a final ΔK (and plastic zone size) at which the actual test could commence without causing crack growth retardation or acceleration. The initial crack length, a_0, was taken as the mean of the precrack lengths as measured on both specimen faces.

Crack lengths at elevated temperatures were measured using the electrical potential difference technique[14] with build-in temperature compensation by automatic computer-controlled reversal of the electrical poles. Four Ni/Cr wires acting as electrical leads were attached to each CT specimen by electrowelding. At room temperature, a video camera with a zoom lens was used to view the crack tip region and measure the crack length. The crack length and the electrical potential at various intervals of number of cycles were recorded during the test. While at elevated temperature, it was difficult to measure the crack length directly, so only the electrical potentials were recorded for determining crack length by electric potential difference (EPD) measurement. The crack length was calculated from EPD using the Hick and Pickard relationship, which has been demonstrated to have high resolution and accuracy for standard fatigue crack length applications[15]. The relationship between EPD and crack length for the CT sample geometry in this study was as follows:

$$a/W = 0.263\,99 - 0.030\,9(\varphi/\varphi_0) + 0.147\,94(\varphi/\varphi_0)^2 - 0.031\,18(\varphi/\varphi_0)^3 \quad (3)$$

where φ is the measured electric potential and φ_0 is the initial electric potential corresponding to $a/W = 0.35$.

In order to find the threshold, an initial load was applied and maintained for a minimum of 8 000 cycles. If there was no crack growth, reflected by change of EPD, after this number of cycle, the load was then increased by an increment not exceeding 2 MPa·$m^{1/2}$. This process was repeated until the crack started advancing. Crack growth rates (CGR) were calculated using 7-point method and plotted as function of ΔK.

In addition, interrupted fatigue crack propagation tests were also performed for microscopic examination of the active zone adjacent to the main crack. The side zone was examined using optical microscope and scanning electron microscope. The fracture surface was also examined using the same procedure.

3 RESULTS AND DISCUSSION

Plots of the crack length, a, versus the number of cycles, N, for K40S alloy examined at 700 ℃ and 900 ℃ are shown in Fig. 1. It can be seen that, at 700 ℃, the total fatigue lifetime is approximately 3×10^5 cycles, while that is 1.5×10^5 cycles at 900 ℃. The initiation lifetime is approximately 2×10^4 cycles at 700 ℃ and 1×10^4 cycles at 900 ℃, respectively. The main propagation lifetime is about 2.8×10^5 cycles and 1.2×10^5 cycles at 700 ℃ and 900 ℃, respectively. The crack grew up to 12 μm after initiation. Both cracks propagated very fast in the last several thousand cycles and the final crack lengths were about 22 mm. The relationship between the crack growth rate, da/dN, and the crack length, a, are shown in Fig. 2. Both curves demonstrate crack growth kinetics of

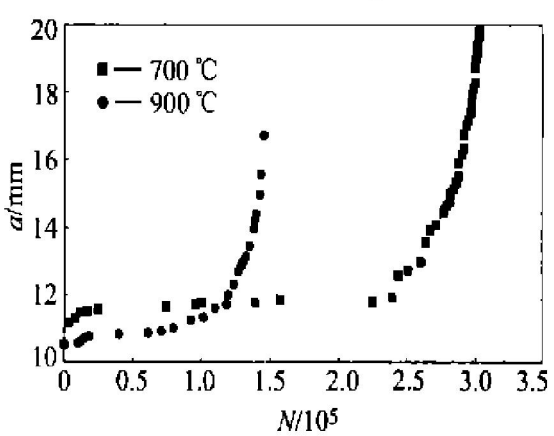

Fig. 1 Plots of fatigue crack length vs number of cycles for K40S alloy

sigmoidal feature, which can be divided into three distinct stages: the crack initiation stage, the stable crack propagation stage and the critical stage. In these stages, the crack growth rate varies appreciably.

The crack growth rate, da/dN, versus the stress intensity factor range, ΔK, for K40S alloy examined at 700 ℃ and 900 ℃ are plotted in Fig. 3. It can be seen that the $da/dN - \Delta K$ curves are also sigmoidal. That is to say that at both the low and high ΔK regions, the crack growth rates increase markedly. At the low ΔK region, the curves approach a vertical asymptote. A fatigue threshold, ΔK_{th} at each temperature can be operationally defined as ΔK at which the crack growth is presumed dormant. It is a critical parameter because components operate close to the fatigue threshold regime for the majority of their lifetime[16]. Below the threshold, the existing cracks in the components would not grow. Therefore, fatigue damage is unlikely. It can be seen from Fig. 3 that K40S alloy shows a well-defined fatigue threshold, i. e. the fatigue thresholds are 23. 9 MPa·$m^{1/2}$ and 12 MPa·$m^{1/2}$ at 700 ℃ and 900 ℃, respectively.

A linear region at an intermediate stress intensity

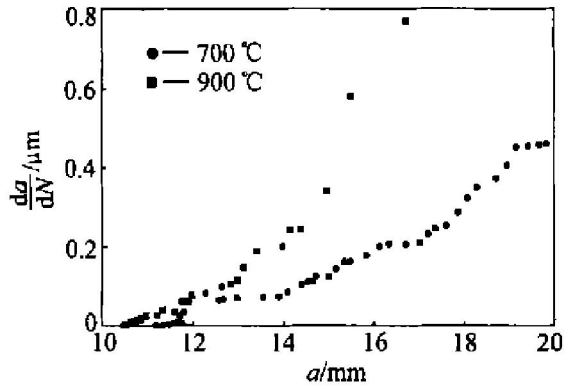

Fig. 2 Plots offatigue crack growth rate vs crack length for K40S alloy

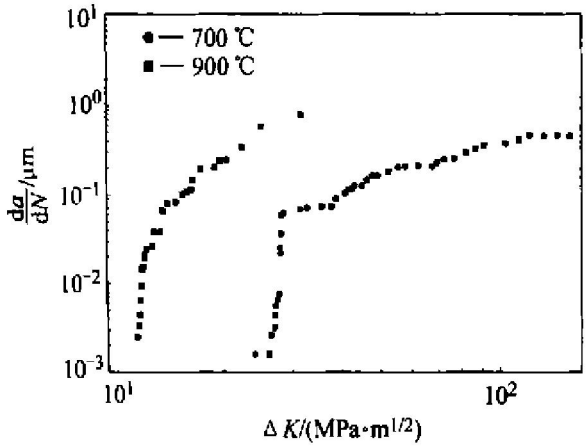

Fig. 3 Plots of fatigue crack growth rate as function of stress intensity range for K40S cobalt-base superalloy (R= 0. 1)

factor range represents stable fatigue crack growth. The relationship between da/dN and ΔK follows the Paris-Erdagan power-law (Eqn. (1)) in such region. Least-squares analysis yielded the two material constants, c and m, which are listed along with the coefficient of determination (R^2) in Table 1. These calculations were performed only with the data having Δa increments of 0. 25 mm. The points in the near threshold regime were not included in this analysis. It can be seen that the R^2 is 0. 94 and 0. 98 respectively, which indicates that it fits the Paris-Erdagan power law well.

Table 1 Parameters of Paris-Erdagan power law relationship for K40S alloy

Temperature/℃	c	m	R^2	ΔK_{th}/(MPa·$m^{1/2}$)
700	6.36×10^{-17}	7.23	0.94	23.9
900	7.53×10^{-19}	6.72	0.98	12.0

As it is known that, just like the fatigue strength, the fatigue threshold is an important fatigue property for structural materials. It is also reported that, the higher the strength, the lower the fatigue threshold is, and the higher the ductility, the higher the fatigue threshold is[17, 18]. The strength and ductility of K40S alloy are listed in Table 2. It can be seen that the ductility of K40S alloy at 900 ℃ is superior. In regards to the ductility and tensile strength points, it seemed that the threshold of K40S alloy at 900 ℃ should be higher than that at 700 ℃. But the result was reverse. Just as mentioned above, the increasing temperature would cause an increase in CGR at a given ΔK under a symmetric sinusoidal loading waveform. In general, the effect of temperature on CGR was attributed to the oxygen environment effect. Due to oxidation layer within the cracks, oxide-induced closure should be more pronounced, thereby reducing the CGR, compared with these of lower temperature[19, 20]. The crack tips are also blunt at higher temperature, which would reduce the crack drive force and impede fatigue crack growth. This behavior plays an important role in retarding fatigue crack growth at low stress ratio R values[21] or near the threshold regime[22]. There is, however, more degradation of the material due to oxygen embrittlement, which may significantly reduce the ΔK required to propagate a crack. A brittle oxide layer at crack tip is formed more easily through enhanced diffusion at elevated temperature and is subsequently fractured by the cyclic stress. The deleterious effects of oxygen at high temperature on fatigue crack propagation were reported in previous studies on DZ40M and MAR-M509 cobalt-base superalloy[23, 24].

Table 2 Tensile properties of K40S alloy

Temperature/ ℃	$\sigma_{0.2}$/ MPa	σ_b/ MPa	δ/ %	Reduction of area/ %
700	259	583.5	15.8	17.8
900	204	248.6	30	41

At 700 ℃, the initial stage contains the fatigue damage features associated with the near-threshold crack propagation, dimples and limited microcracks, microvoids, as shown in Fig. 4(a). These features indicate a ductile fracture mechanism related to the initial stage of crack growth. With an increase of temperature from 700 ℃ to 900 ℃, the appearance on fractograph is identical except for heavier oxidation, as shown in Fig. 4(b).

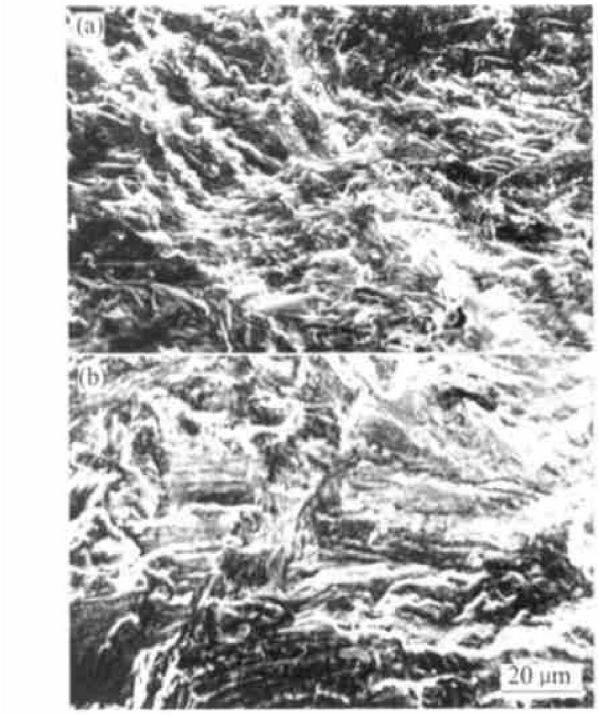

Fig. 4 SEM micrographs of K40S alloy at crack initiation stage
(a) —700 ℃; (b) —900 ℃

The mid-stage region is the stable crack propagation region. At 700 ℃, this region is characterized by cleavage, interdendritic separation, tearing ridges and microcracks. Such features can be found in Fig. 5(a). The brittle nature of primary carbide and its poor combination with the substrate weaken the microstructure continuation, which results in its separation from the matrix under the alternating load. While at 900 ℃, the primary carbide is oxidized preferentially (as shown in Fig. 5(b)), which results in accelerating the crack propagation. These features shown in Fig. 5 reflect the crack deceleration and indicate that a considerably high energy consuming process is associated with crack propagation.

The final stage is characterized by fast crack propagation features, such as interdendritic separation (as shown in Fig. 6(a) and (b)). In high stress intensity factor range, microvoids are visible on the fracture surfaces of the samples, which indicates a high ductility of the microstructure under such test condition.

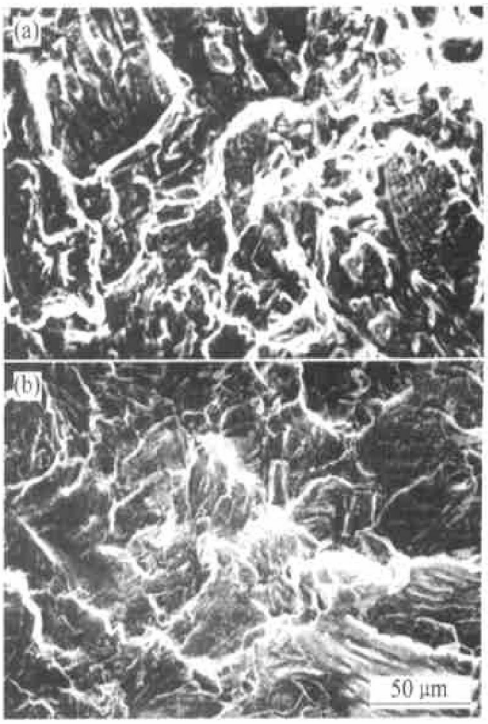

Fig. 5 SEM micrographs of K40S alloy at stable crack propagation stage
(a) —700 ℃; (b) —900 ℃

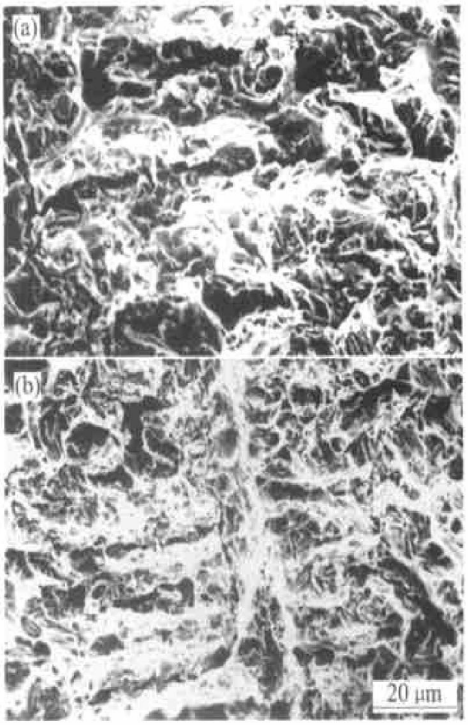

Fig. 6 SEM micrographs of K40S alloy at critical final stage
(a) —700 ℃; (b) —900 ℃

4 CONCLUSIONS

1) Under ambient atmosphere, there is a well defined threshold for K40S alloy at elevated temperatures. The fatigue threshold is 23.9 MPa·$m^{1/2}$ at 700 ℃ and 12 MPa·$m^{1/2}$ at 900 ℃.

2) The significant decreasing ΔK with the increasing temperature is associated with the oxidation induced embrittlement at crack tip.

3) The fracture surface morphology shows dimples indicating the ductile failure mechanism in the near threshold or initiation stage. The stable crack growth region displays intensive tearing ridges, microcracks and cleavages indicating a high energy dissipation process. The unstable growth region displays interdendritic separation.

REFERENCES

[1] Beltran A M, Sims C T. The high temperature properties of MAR-M509 alloy [J]. J Met, 1969, 21(9): 39 - 47.

[2] Sims C T, Hagel W C. The Superalloy [M]. New York: John Willy & Sons Inc, 1992.

[3] YUAN F H. High Temperature Corrosion and Oxidation Behavior of a Cobalt Base Superalloy [D]. Institute of Metal Research, Chinese Academy of Sciences, 1999.

[4] Filling code Co-8 stellite alloy No. 31 [R]. Alloy Digest, Upper Montclair. New Jersey: Engineering Alloy Digest Inc, 1956.

[5] Subramanian P R, Mendiratta M G, Dimiduk D M. The development of Nb-base advanced intermetallic alloy for structural application [J]. J Met, 1996, 48(1): 33 - 38.

[6] Soboyejo W O, Dipasquale J, Ye F, et al. An investigation of the fatigue and fracture behavior of a Nb-12Al-44Ti-1.5Mo intermetallic alloy [J]. Metall Trans, 1999, A30: 1025 - 1038.

[7] Aglan H, Gan Y X. Fatigue crack growth analysis of a premium rail steel [J]. J Mater Sci, 2001, 36(2): 389 - 397.

[8] ZHANG Jie-ping. Fatigue crack propagation behavior of underfill materials in microelectronic packaging [J]. Mater Sci Eng, 2001, A314: 194 - 200.

[9] Paris P C, Erdogan F. Crack growth laws for the characterization of fatigue cracks [J]. Trans ASMT, J Basic Eng, 1963, 85: 528 - 534.

[10] Standard Test Method for Measurement of Fatigue Crack Growth Rates E647-95a [S]. Annual Book of ASTM Standards[M]. Philadelphia PA ASTM, 1996, 565 - 601.

[11] Campbell J P, Rao K T, Ritchie R O. The effect of microstructure on fracture toughness and fatigue crack growth behavior in gamma-titanium aluminide based intermetallics [J]. Metall Trans, 1999, A30(3): 563 - 575.

[12] Pearson S E. Effect of mean stress on fatigue crack propagation in half Inch and 12.7 mm thick specimens of Al alloys of high and low fracture toughness [J]. Eng Fract Mech, 1972, 4: 9 - 24.

[13] Branco C M, Radon J C, Culver L E. Analysis of the influence of mean stress intensity and environment on fatigue crack growth in a new high strength Al alloy [J]. ASTM J Test Eval, 1975, 3(6): 195 - 209.

[14] Donald J K, Ruschau J. Direct current potential difference fatigue crack measurement techniques [A]. Marsh K J, Smith R A, Ritchie R O Eds. Fatigue Crack Measurement [M]. London: Pergamon Press, 1989, 11 - 37.

[15] Hick M A, Pickard A C. A comparison of theoretical and experimental methods of calibrating the electrical potential drop technique for crack length determination [J]. Int Journal of Fracture, 1982, 20: 91 - 101.

[16] Dauskardt H R, Kook S Y, Kirtikar A, et al. Soboyejo W O, Srivatsan T S. Proceedings of Symposium of High Cycle Fatigue of Structural Materials [C]. The Minerals Metals and Materials Society, 1997. 479 - 498.

[17] Robinson J C. Fatigue and Microstructure [M]. Ohio: ASM Metal Park, 1979, 245.

[18] Irving P E. Fatigue and Microstructure [M]. Ohio: ASM Metal Park, 1979, 254.

[19] Suresh S, Zamiski G F, Ritchie R O. Oxide-induced crack closure: an explanation for near-threshold corrosion fatigue crack growth behavior [J]. Metall Trans, 1981, A12(8): 1435 - 1443.

[20] Liaw P K, Saxena A, Swaminathan V P, et al. Effects of load ratio and temperature on the near-threshold fatigue crack propagation behavior in a CrMoV steel [J]. Metall Trans, 1983, A14(8): 1631 - 1640.

[21] Matuszyk W, Camus G, Duquete D J, et al. Effects of temperature and environment on the tensile and fatigue crack growth behavior of a Ni_3Al base alloy [J]. Metall Trans, 1990, A21(11): 2967 - 2980.

[22] Zhang G P, Wang Z G, Li G Y. Fatigue crack growth of Ni_3Al(CrB) single crystals at ambient and elevated temperatures [J]. Acta Mater, 1997, 45(4): 1705 - 1714.

[23] Jiang W H, Yao X D, Guan H R, et al. High temperature fatigue of a directionally solidified cobalt-base superalloy [J]. Acta Metall Sin, 1998, 11(4): 111 - 115.

[24] Reuchet J, Remy L. High temperature low cycle fatigue of MAR-M509 superalloy [J]. Mater Sci Eng, 1983, 58: 19 - 42.

(Edited by YANG Bing)